2D Materials

Magnetism and Spin Dynamics in Room-Temperature van der Waals Magnet Fe_5GeTe_2

To cite this article before publication: Laith Alahmed *et al* 2021 *2D Mater.* in press https://doi.org/10.1088/2053-1583/ac2028

Magnetism and Spin Dynamics in Room-Temperature van der Waals Magnet Fe_5GeTe_2

Laith Alahmed,[†] Bhuwan Nepal,[‡] Juan Macy,[¶] Wenkai Zheng,[¶] Brian Casas,[¶] Arjun Sapkota,[‡] Nicholas Jones,[†] Alessandro R. Mazza,[§] Matthew Brahlek,[§] Wencan Jin,[∥] Masoud Mahjouri-Samani,[†] Steven S.L. Zhang,[⊥] Claudia Mewes,[‡] Luis Balicas,[¶] Tim Mewes,[‡] and Peng Li*[,†]

†*Department of Electrical and Computer Engineering, Auburn University, Auburn, AL 36849*

‡*Department of Physics, University of Alabama, Tuscaloosa, AL 35487*

¶*National High Magnetic Field Laboratory, Florida State University, Tallahassee, Florida 32310*

§*Materials Science and Technology Division, Oak Ridge National Laboratory, Oak Ridge, TN, 37831, USA*

∥*Department of Physics, Auburn University, Auburn, AL 36849*

⊥*Department of Physics, Case Western Reserve University, Cleveland, Ohio 44106*

E-mail: wzj0029@auburn.edu,sxz675@case.edu,tmewes@ua.edu,balicas@magnet.fsu.edu, pzl0047@auburn.edu

Abstract

Two-dimensional (2D) van der Waals (vdWs) materials have gathered a lot of attention recently. However, the majority of these materials have Curie temperatures that

are well below room temperature, making it challenging to incorporate them into device applications. In this work, we synthesized a room-temperature vdW magnetic crystal Fe_5GeTe_2 with a Curie temperature $T_c = 332$ K, and studied its magnetic properties by vibrating sample magnetometry (VSM) and broadband ferromagnetic resonance (FMR) spectroscopy. The experiments were performed with external magnetic fields applied along the c-axis ($H \| c$) and the ab-plane ($H \| ab$), with temperatures ranging from 300 K to 10 K. We have found a sizable Landé g-factor difference between the $H \| c$ and $H \| ab$ cases. In both cases, the Landé g-factor values deviated from $g = 2$. This indicates contribution of orbital angular momentum to the magnetic moment. The FMR measurements reveal that Fe_5GeTe_2 has a damping constant comparable to Permalloy. With reducing temperature, the linewidth was broadened. Together with the VSM data, our measurements indicate that Fe_5GeTe_2 transitions from ferromagnetic to ferrimagnetic at lower temperatures. Our experiments highlight key information regarding the magnetic state and spin scattering processes in Fe_5GeTe_2, which promote the understanding of magnetism in Fe_5GeTe_2, leading to implementations of Fe_5GeTe_2 based room-temperature spintronic devices.

I. Introduction

The increasing interest in magnetic two-dimensional (2D) van der Waals (vdWs) materials in recent years is warranted by their importance for fundamental studies of 2D magnetism, as well as potential applications for spintronic devices. Compared to three-dimensional (3D) magnets, 2D magnetic materials exhibit exotic electrotransport, optical, and spin properties.[1–3] One of the biggest practical issues of most 2D vdWs magnetic materials is that they generally have a Curie temperature (T_c) that is well below room temperature, making it difficult to incorporate them into relevant devices.[4–9] For example, the Curie temperatures of 2D magnetic materials such as $Cr(Si,Ge)Te_3$ (33 K and 61 K),[4,5] and $Cr(Br,I)_3$ (47 K and 61 K),[6,7] are all lower than typical 3D magnets. This is due to their 2D nature, where the

pair-exchange interaction is much weaker than in 3D magnets, as it is mostly mediated by neighboring magnetic atoms in the 2D plane.

The low T_c of the aforementioned 2D vdWs ferromagnets makes it impossible to use them in room-temperature spintronic devices. More specifically, in the 2D limit, it was shown theoretically that the Curie temperature is given by the uniaxial magnetic anisotropy constant K, and the spin-exchange interaction J, as follows:[10]

$$T_c \sim \frac{4\pi J}{3ln(\pi^2 J/K)} \tag{1}$$

According to Equation (1), as the magnetic anisotropy in vdWs ferromagnets is much smaller than the exchange interaction, T_c is low.[11] It should be noted that the Fe_5GeTe_2 compound has a complex crystalline structure with more than one inequivalent iron positions. Thus, this equation only gives a crude estimation of T_c. Extensive research efforts succeeded in engineering 2D materials that could overcome these challenges. For example, T_c can be significantly raised to about room temperature by enhancing exchange interaction while keeping the vdWs structure,[11] such as in the layered 2D Fe_nGeTe_2 ($n \geq 3$).[12,13] This led to Fe_3GeTe_2 with T_c around 220 K,[9,14,15] Fe_4GeTe_2 with $T_c = 270$ K,[11] and Fe_5GeTe_2 with T_c ranging from 260 - 310K, depending on the Fe content.[13,16,17]

Fe_5GeTe_2 was first synthesized by May et al. who found that its Curie temperature is $\sim$ 310 K.[16,17] It was later discovered that Fe_5GeTe_2 possesses itinerant long-range ferromagnetism,[13] which originates from the giant spin polarization of the delocalized ligand Te states.[18] A recent work reported that Fe_5GeTe_2 transitions from ferromagnetic to ferrimagnetic at 275 K, and then to glassy clusters as the temperature reduces to 100 K.[19] Besides, several groups carried out electro-transport measurements and detected anomalous and topological Hall effects.[19,19–21,21] The magnetization dynamics in Fe_5GeTe_2, however remain unexplored, and thus is the focus of this work.

Ferromagnetic resonance (FMR) spectroscopy is an important technique to study mag-

netization dynamics.[22,23] Several studies have analyzed the spin dynamics in 2D magnets by FMR,[24–26] which revealed their magnetocrystalline anisotropy dependence on temperature. It is found that there is a discrepancy between the Landé g-factor along the c-axis and the ab-plane directions in the 2D magnet $Cr_2Ge_2Te_6$.[26,27] However, the Landé g-factor is quite isotropic along different directions in another 2D magnet CrI_3.[25] These measurements were all performed on 2D magnets with low Curie temperatures (e.g. $T_c = 61$ K for CrI_3). With the most promising room-temperature vdWs magnet arguably being Fe_5GeTe_2, we are interested in understanding its quasi-static and dynamic magnetic properties, which can shed light on its magnetic states and spin scattering mechanisms.

We first synthesize the vdWs magnet Fe_5GeTe_2, and then we study its magnetization properties using both vibrating sample magnetometry (VSM) and ferromagnetic resonance (FMR) spectroscopy, in the temperature range of 300 K to 10 K. For FMR, a microwave field was applied to the sample in addition to a quasistatic magnetic field, thus triggering spin precession. At the resonance field H_{res} for a given microwave frequency f, FMR oscillations (uniform-mode excitation with $k \approx 0$) occur. The FMR spectroscopy has revealed different Landé g-factors along the c-axis and the ab-plane in Fe_5GeTe_2, indicative of orbital moment contribution to the magnetic moment. After examining the temperature dependence of the FMR linewidth, we find that Fe_5GeTe_2 has an effective damping coefficient similar to Permalloy at room temperature. The increased FMR linewidth at lower temperatures indicates that Fe_5GeTe_2 experiences a magnetic phase transition from ferromagnetism to ferrimagnetism.

II. Structure Characterization

Nominal Fe_5GeTe_2 crystals are grown using a mixture of precursor materials filled into a quartz ampoule that is vacuumed and sealed with 1.9 mg/cm^3 of iodine as a transport agent. The mixture consists of pure elements of Fe:Ge:Te in the molar ratio of 6.2:1:2 (Fe:

99.998%, powder, Alfa Aesar; Ge: 99.999%, 100 mesh, Alfa Aesar; Te: 99.999%, powder, Alfa Aesar). The excess Fe powder is to compensate for any possible Fe-site vacancies that might occur during the growth.

A standard MTI 2-zone model OTF-1200X furnace was employed, where the reactants or elemental precursors were placed in the high-temperature zone and the products were grown in the low-temperature side. The ramping rate for both the hot (775 °C) and cold (700 °C) zones to their target temperatures was 1 °C/min. This temperature differential was held for 14 days with the Fe_5GeTe_2 crystals being subsequently quenched in an ice bath.

Prior to characterization, the excess iodine was removed through a bath and rinse cycle of acetone and isopropyl alcohol, respectively. Samples were either stored in a glove box with high purity argon gas (99.99%) of 0.01 ppm O_2/H_2O, or a desiccator under vacuum with pressures ranging between 100-200 mTorr.

The following results are obtained from a bulk Fe_5GeTe_2 crystal in the shape of an ellipse, with area = 3.2×10^{-3} cm^2 and thickness $\sim$ 100 microns. The crystalline structure characterization is presented in Figure 1. Figure 1a shows the crystal structure schematic of Fe_5GeTe_2. The vdW-separated eight atomic-thick monolayers of two unit cells can be observed, where the vdWs gaps exist between the Te atoms of neighboring unit cells. The light-blue circles labeled Fe(1) represent the two possible occupation locations for the Fe(1) atoms, either above or below a given Ge atom, with an occupation probability not exceeding 50%, as the Fe-Ge bond becomes non-physical if both locations are occupied simultaneously.[16]

The X-ray diffraction (XRD) data collected for the experimental Fe_5GeTe_2 sample crystal are shown in Figure 1b. The $(00l)$ reflections reveal the c-axis of the single crystal. The $(00l)$ peaks, where l=3n, reflect an ABC stacking sequence in the unit cell of the bulk crystal. This is consistent with the rhombohedral lattice structure of the R3m (No. 166) space group, as previously reported.[13,16]

The rocking curves measured at $(00l)$ peak angles are shown in Figure 1c. The full-width-at-half-maximum values of the acquired curves, with values less than 0.06°, reflect the

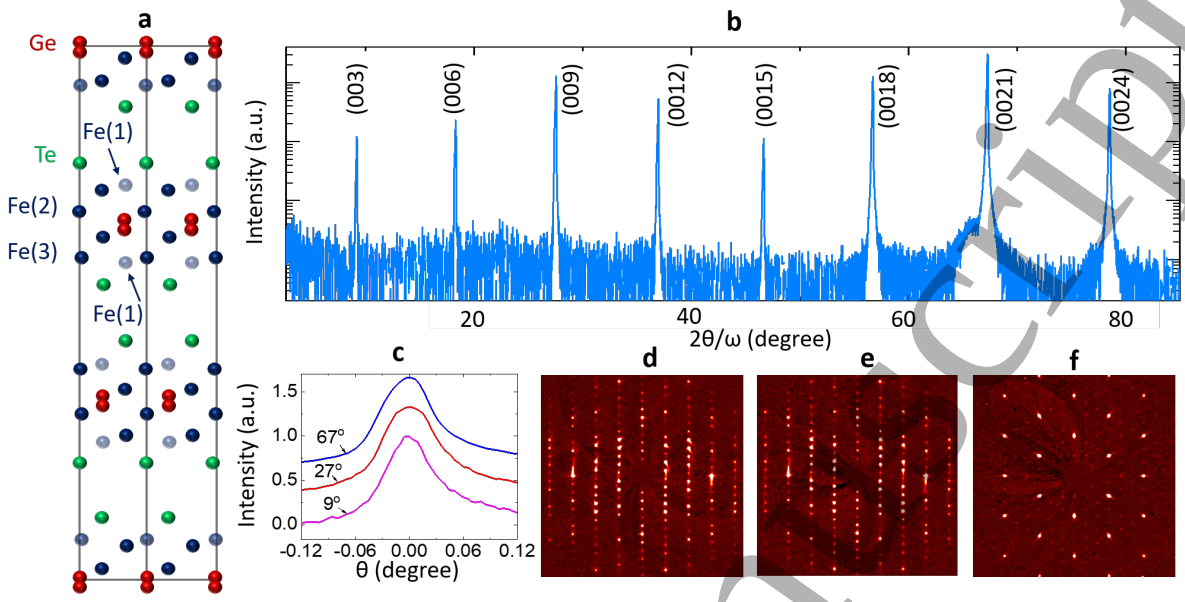

Figure 1: Crystal structure and x-ray diffraction (XRD) of single crystal Fe_5GeTe_2. **a**. Schematic of crystal structure of Fe_5GeTe_2. **b**. XRD $2\theta/\omega$ scan showing $(00l)$ peaks. **c**. Rocking curve scan of the peaks at 9°, 27°, 67° showing high crystallinity. **d-f**: Single crystal XRD scan of Bragg reflections of different planes. **d**: $(0kl)$ plane. **e**: $(h0l)$ plane. **f**: $(hk0)$ plane.

high level of crystallinity of the Fe_5GeTe_2 samples. Figures 1d-f are Bragg reflection scans of different crystal planes $(0kl)$, $(h0l)$, $(hk0)$ from high-resolution XRD. They all show clear streaks, confirming the high-quality of the single-crystal samples.

III. Quasi-Static Magnetization Properties

Quasi-static magnetization properties were measured using VSM in a Quantum Design Dynacool PPMS system. The measurements were carried out with the magnetic field applied along both the c-axis ($H \| c$) and the ab-plane ($H \| ab$) directions. To determine the Curie temperature of the sample, we measured field-cooled curves, as well as heat capacity curves in the absence of a magnetic field.

Figure 2a shows the results of the VSM magnetization versus field measurements of the Fe_5GeTe_2 sample, for temperatures ranging from 1.8 K to 350 K, and external field applied along both the c-axis (dashed lines) and the ab-plane (solid lines) directions. The

curves show that the easy-axis of Fe_5GeTe_2 is in-plane because a stronger field is required to saturate the sample along the c-axis, compared to the ab-plane, at all temperatures. Further measurements (See Supplementary Material Section I) show that there is no uniaxial anisotropy within the ab-plane, establishing Fe_5GeTe_2 as an easy-plane magnet. Possible spin-reorientation features, such as the ones observed in Fe_4GeTe_2,[11] are not observed in this sample. Our results are reasonable considering the fact that the out-of-plane magnetocrystalline anisotropy in Fe_5GeTe_2 crystals is weak.[11,19] Figure 2b shows the field-cooled (FC) curves for the $H \| c$ and the $H \| ab$ cases. The magnetization magnitude change on the $H \| ab$ curve indicates a possible magnetic phase transition. This feature has been reported in previous publications.[11,16,19] Based on the transition points of the FC curves, the Curie temperature was estimated to be $T_c = 332 \pm 5$ K.

Heat capacity measurements were used to validate the Curie temperature estimation. The measurements were set to start from the highest temperature setpoint, $T = 390$ K, then the temperature was gradually reduced to 1.8 K as the heat capacity data was collected. This procedure guarantees that an appropriate time constant is used to achieve more stable readings. The measurement results are shown in Figure 2c. Two points of interest are highlighted on the curve by two black arrows. The first is a transition at $T = 332$ K, which is consistent with T_c from the FC measurement. The second is the observation of a slope change around $T = 110$ K. The slope change again indicates that Fe_5GeTe_2 experiences some phase transition, which will be discussed more extensively in the analysis of FMR linewidth in Section IV.

IV. Magnetization Dynamics

We measured the FMR response of the Fe_5GeTe_2 sample for $H \| c$ and for $H \| ab$, at temperatures varying from 10 K to 300 K. In our custom-built system, a coplanar waveguide (CPW) with impedance matched to 50 Ω was used to guide the microwave field to the sample.

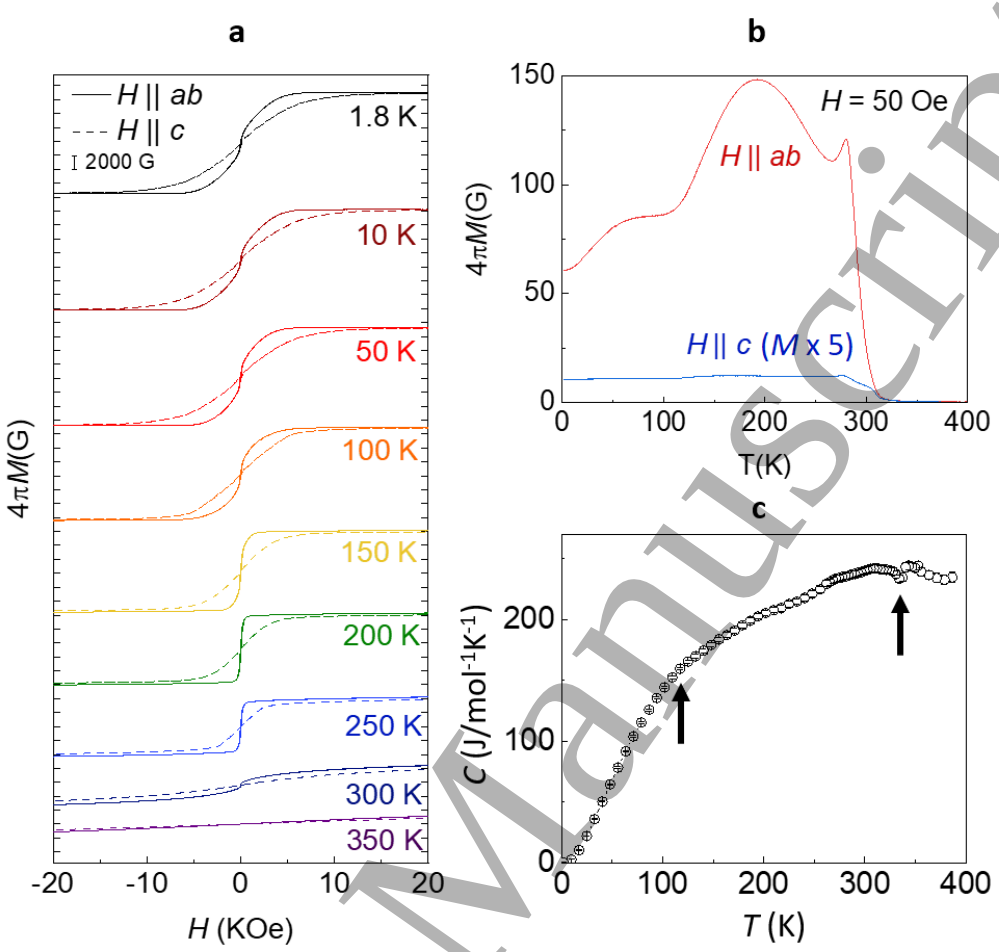

Figure 2: Static magnetization of the Fe_5GeTe_2 bulk single crystal. **a**. Temperature-dependent hysteresis loops at various temperatures for $H \| c$ (dashed lines) and $H \| ab$ (solid lines). **b**. Field-cooled curves ($H = 50$ Oe) for the $H \| c$ (blue) and the $H \| ab$ (red) cases, respectively. **c**. Heat capacity as a function of temperature. The transition at 332 K and 110 K mark the Curie temperature and possible magnetic phase transition, respectively.

The tested microwave frequencies ranged from 5 GHz to 40 GHz, with higher frequencies up to 115 GHz used in the room temperature $H \| c$ case, along with high magnetic fields, to ensure that the magnetization of the sample is fully saturated at FMR. For each microwave frequency, the magnetic field was swept from high magnetic field towards zero. A microwave diode was used to convert the transmitted microwave signal to a dc voltage. To improve the signal-to-noise ratio, we used a set of field-modulation coils supplemented by a lock-in amplifier to detect the signal. Thus, the detected FMR response is identified as the derivative of the microwave power absorption.

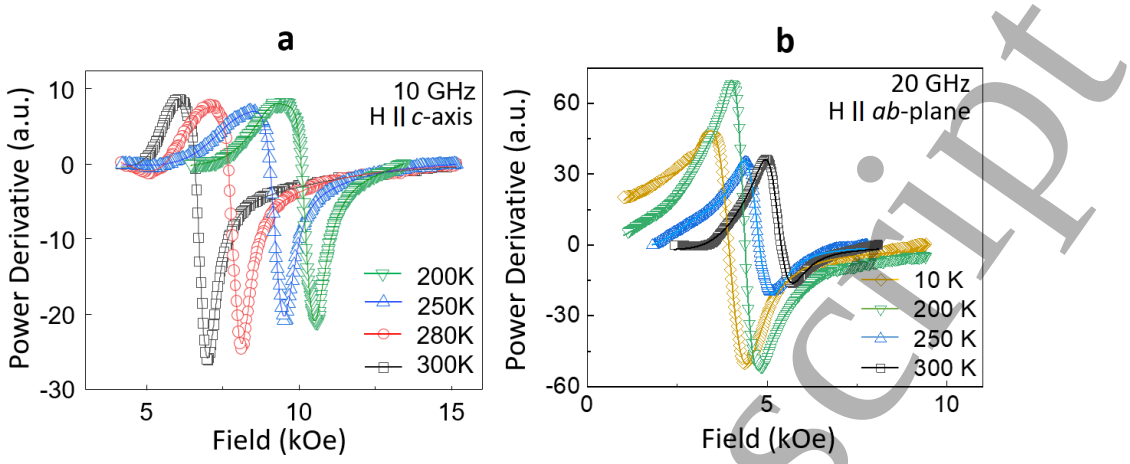

Figure 3: Ferromagnetic resonance (FMR) measurements of Fe_5GeTe_2 single crystal. **a**. FMR profiles for $H \| c$ at 200 K, 250 K, 280 K, and 300 K. **b**. FMR profiles for $H \| ab$ at 10 K, 200 K, 250 K and 300 K.

As shown in Figure 3, we detected strong FMR responses at 300 K, demonstrating ferromagnetism of Fe_5GeTe_2 at room temperature. Figures 3a and 3b show the temperature dependence of the FMR profiles at 10 GHz and 20 GHz, for $H \| c$ and $H \| ab$, respectively. Besides the data points, the curves show fits to the derivative of a combination of symmetric and antisymmetric Lorentzian functions.[22] The measured FMR response is a time-averaged signal of the microwave power absorption. Such absorption is dispersive and has a symmetric feature. However, there are a number of effects, including Eddy currents, that can lead to a phase shift of the driving microwave field relative to the original signal.[28] Such a phase shift leads to a quadrature component that manifests as an antisymmetric contribution to the FMR signal.[29,30] From the fits, one can extract the resonance field H_r and peak-to-peak linewidth ΔH_{pp} as shown in Figures 4 and 5, respectively. It is observed that the magnitude of the FMR peaks decays with reducing temperature in the $H \| c$ case. Below 200 K, the FMR signal becomes undetectable in this orientation. We attribute this phenomenon to the broadening of the FMR resonance peaks.

The resonance frequencies f vs. the FMR resonance fields H_{r} at different temperatures are plotted in Figures 4a and 4b for the $H \| c$ and for the $H \| ab$ cases, respectively. The

fitting equation for the $H \| c$ measurements is:[31]

$$f = \gamma'(H_r - 4\pi M_{\text{eff}}) \tag{2}$$

and the fitting equation for the $H \| ab$-plane measurements is:[31]

$$f = \gamma' \sqrt{(H_r + 4\pi M_{\text{eff}}) H_r} \tag{3}$$

where f is frequency, γ' is the reduced gyromagnetic ratio ($\gamma' = \frac{|\gamma|}{2\pi}$), and $4\pi M_{\text{eff}}$ is the effective magnetization. The fitted curves are also presented in Figures 4a and 4b. By fitting the data with equations (1) and (2), we obtain different γ' and corresponding spectroscopic Landé g-factor values, as well as M_{eff} values, for the $H \| c$ and $H \| ab$ cases, as shown in Figures 4c and 4d, respectively. We note that the $4\pi M_{\text{eff}}$ values obtained along those two orientations are in good agreement with each other. A difference between these two values could be an indication for the presence of a higher order anisotropy,[32] but this is not the case here. In Figure 4c, the left vertical axis shows γ', and the right vertical axis shows the Landé g-factor calculated using $|\gamma| = g\frac{\mu_B}{\hbar}$. The g-factor exhibits a weak dependence on temperature along both the ab-plane and the c-axis directions. However, it deviates from g = 2.

Furthermore, our data appears to indicate a sizable difference of the g-factor along different directions in Fe_5GeTe_2. Similar to $Cr_2Ge_2Te_6$,[26] the deviation of the g-factor from g = 2 may suggest an orbital contribution to the magnetization due to spin-orbit coupling in Fe_5GeTe_2. It was found that strong spin-orbit coupling results in nontrival Berry phase in Fe_3GeTe_2, another member in the Fe_nGeTe_2 ($n \geq 3$) family. In this case, the orbital character is formed by a mixture of 3D orbitals from the Fe I–Fe I dumbbells and Fe II sites.[33] A theoretical work found that the magnons can have long lifetimes and exhibit nonreciprocal magnon transport in Fe_3GeTe_2.[34] In Fe_5GeTe_2, the spin-orbit coupling could be characterized by the d orbitals of Fe atoms and p orbitals of Te atoms.[26] In addition, the

anisotropy of the g-factor, which follows from that of the orbital moment, is also expected physically: a small orbital moment arising from reduced crystalline symmetry may "lock" the large isotropic spin moment into its favorable lattice orientation through spin-orbit coupling, giving rise to a sizable magnetic anisotropy. Therefore, it is likely that the orbital moment is closely linked to the magnetocrystalline anisotropy in itinerant ferromagnets, as shown theoretically by Bruno et al.[35] for transition-metal monolayers. A recent experiment used x-ray magnetic circular dichroism (XMCD) and detected the contribution of the orbital moment to the overall magnetization of Fe_5GeTe_2.[18]

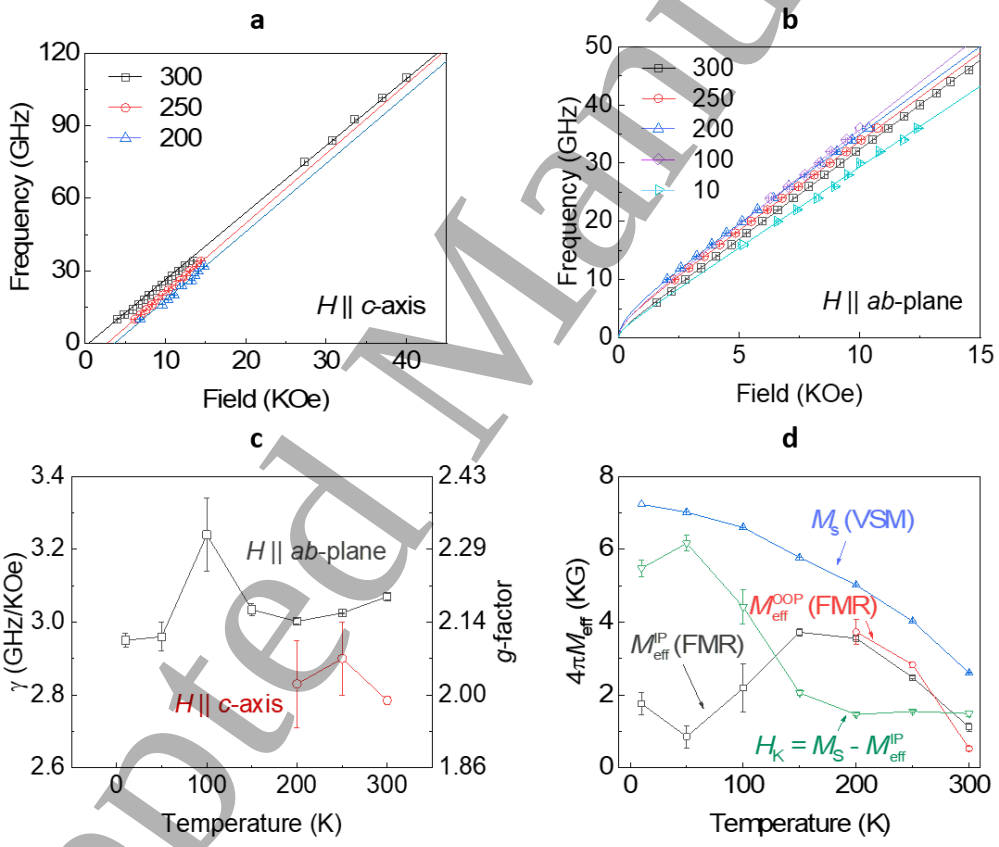

Figure 4: Analysis of the FMR data of the Fe_5GeTe_2 single crystal. **a**. Frequency f vs. resonance field H_r at 200 K, 250 K, and 300 K for $H \| c$. The data points are fitted to Eq. (2). **b**. Frequency f vs. resonance field H_r at 10 K, 100 K, 200 K, 250 K, and 300 K for $H \| ab$. The data points are fitted to Eq. (3). **c**. Temperature dependence of the gyromagnetic ratio γ and spectroscopic g-factor for the $H \| c$ (red) and $H \| ab$ (black) cases, respectively. **d**. Temperature dependence of saturation magnetization $4\pi M_s$ and effective magnetization $4\pi M_{eff}$ from VSM and FMR measurements, respectively.

It is worth noting that an unsaturated magnetization at FMR can also lead to an inaccurate estimation of the gyromagnetic ratio.[36] Because the c-axis magnetization saturates at significantly larger magnetic fields, it is possible that the magnetization was not fully saturated for FMR measurements up to 40 GHz. To estimate to first order the influence of an unsaturated sample at resonance, we write $4\pi M_{\rm eff}(H) = 4\pi M_{\rm eff,0} + 4\pi p H$, where H is the external field, $4\pi M_{\rm eff,0}$ is the effective magnetization extrapolated to zero field, and $4\pi p$ is the slope of $4\pi M_{\rm eff}$ vs. H curve in the region where FMR occurs. Using this equation, equation (2) can be written as: $f = \gamma'_{\rm meas}(H_r - 4\pi M_{\rm eff,meas})$, with $\gamma'_{\rm meas} = \gamma'(1 - 4\pi p)$ and $4\pi M_{\rm eff,meas} = \frac{4\pi M_{\rm eff}}{1-4\pi p}$. To exclude this possibility and to comfirm the g-factor anisotropy, we used a high-frequency, high-magnetic-field setup for the FMR measurement (Supplementary Material Section III). The resulting g-factor extracted from the high-field FMR data still shows significant difference between the ab-plane and c-axis, as shown in Figure 4c. Thus, supporting the presence of a g-factor anisotropy in Fe_5GeTe_2.

The fits also yield the effective magnetization $4\pi M_{\rm eff}$ at different temperatures. Figure 4d plots $4\pi M_{\rm eff}$ for both $H\|c$ (i.e., $4\pi M_{\rm eff}^{H\|c}$) and $H\|ab$ (i.e., $4\pi M_{\rm eff}^{H\|ab}$) cases measured from FMR, along with the saturation magnetization $4\pi M_{\rm s}$ measured from VSM. One can see (1) $4\pi M_{\rm eff}^{H\|c}$ and $4\pi M_{\rm eff}^{H\|ab}$ are close, and (2) there is a difference between $4\pi M_{\rm s}$ and $4\pi M_{\rm eff}$. This reveals a crystalline anisotropy field that can be calculated by $H_{\rm k} = 4\pi M_{\rm s}$ - $4\pi M_{\rm eff}^{H\|ab}$. As plotted in Figure 4d, $H_{\rm k}$ is positive and reduces with increasing temperature. This shows that there exists an out-of-plane crystalline anisotropy field $H_{\rm k}$ of several kOe, though it is smaller than the in-plane shape anisotropy. This observation is consistent with previous reports.[11,19]

Next, we analyze the FMR linewidth in order to gain insights on the spin scattering mechanisms in Fe_5GeTe_2. In Figures 5a and 5c, we plot the peak-to-peak linewidth $\Delta H_{\rm pp}$ vs. frequency at different temperatures measured for the $H\|ab$ and the $H\|c$ cases, respectively. For an ideal magnetic thin film that is homogeneous and defect-free, the linewidth reflects intrinsic FMR damping. In this scenario, the uniform magnon mode (k = 0, ferro-

magnetic resonance) decays into Stoner excitations as temperature decreases. This involves the transition of an electron from an occupied state to an unoccupied state of the same wave-vector, which can be described by the interband term in Kambersky's formula.[37,38] It should be noted that Kambersky's model is only appropriate to second order in spin-orbit coupling parameter ξ, but to higher order no intraband terms occur.[39] Besides intrinsic damping, due to non-uniform magnetization states and defects in the sample, the linewidth can be broadened by extrinsic scattering mechanisms such as inhomogeneous line broadening ΔH_0 and two-magnon scattering ΔH_{TMS}. Thus, the FMR linewidth ΔH_{pp} can be expressed by the following form:[40]

$$\Delta H_{\mathrm{pp}} = \frac{2\alpha_{\mathrm{eff}}}{\sqrt{3}|\gamma|}\frac{f}{2\pi} + \Delta H_0 + \Delta H_{\mathrm{TMS}} \tag{4}$$

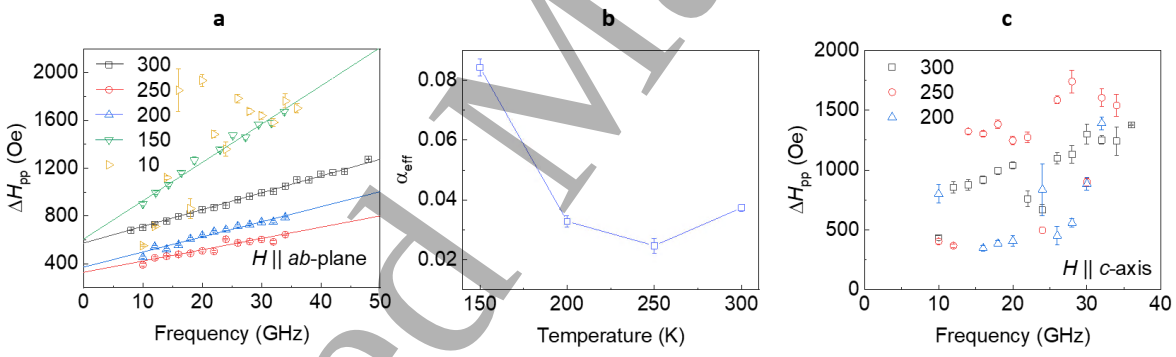

Figure 5: Characterization of FMR linewidth in Fe_5GeTe_2. **a**. Peak-to-peak linewidth ΔH_{pp} vs. frequency for $H \| ab$. **b**. Temperature dependence of effective damping parameter α_{eff} for $H \| ab$. **c**. ΔH_{pp} vs. frequency for $H \| c$.

Figures 5a,c plot the FMR linewidth versus frequency for $H \| ab$ and $H \| c$ cases, respectively. We measured linewidths with the magnitude between 400 Oe to 2000 Oe for both cases. As shown in Figure 5a, the FMR linewidth increases when the temperature reduces from 300 K to 150 K. The linewidth becomes higher and very scattered below 150 K. This indicates extrinsic contributions in Fe_5GeTe_2 at lower temperatures. A previous study showed that when FeRh transitions from ferromagnetic to antiferromagnetic, this causes a significant increase of the FMR linewidth.[41] Other studies have shown a significant increase of the

linewidth in magnetite as it undergoes the Verwey transition,[42] and of the effective damping in Py/Gd bilayers when approaching the Gd ordering temperature.[36] It is likely that the increased linewidth we have observed can also arise from similar magnetic phase transitions. In fact, Ref.[19] has proposed that Fe_5GeTe_2 transitions from ferromagnetic to ferrimagnetic at 275 K, and then transitions to a state with glassy clusters below 110 K. While our AC susceptibility results show no indication of a state with glassy clusters (Supplementary Material Section II), our low-temperature FMR measurements support the argument of ferromagnetic to ferrimagnetic transitions at lower temperatures. We acknowledge that Fe_5GeTe_2 has a very intriguing and complex magnetism and we believe that a complete understanding will require many further studies.

The FMR measurements have shown that Fe_5GeTe_2 exhibits a similar damping constant to that of soft 3D magnets, when interpreting the slope of the linewidth as an effective Gilbert damping parameter. As can be seen from Figure 5b, the effective damping parameter α_{eff} ranges from 0.025 to 0.085 as temperature reduces from 300 K to 150 K. We summarized table 1 for a comparison of the Gilbert damping constant for typical materials. It can be seen that the reported vdW magnets have similar damping constants as 3D magnets. The α_{eff} of Fe_5GeTe_2 is similar to that of soft 3D transition metal magnets such as Permalloy.[43] Because the α_{eff} of Fe_5GeTe_2 is estimated from the $H \| ab$ measurements, it is likely that ΔH_{TMS} also contributes to α_{eff}.

Table 1: Summary of measured effective Gilbert damping constants for different materials at different temperatures.

Material	**type**	**Gilbert damping constant**	**Temperature**	**Source**
NiFe (permalloy) thin film (3 nm)	3D-conducting	0.013	300 K	Ref.[43]
Fe_5GeTe_2	2D-conducting	0.035	300 K	This work
Fe_5GeTe_2	2D-conducting	0.007	10 K	This work
$CrBr_3$	2D-insulating	0.009	30 K	Ref.[44]
$Cr_2Ge_2Te_6$	2D-insulating	0.01-0.08	10 K	Ref.[27]

Summary and conclusion

In summary, we have synthesized a vdWs Fe_5GeTe_2 crystal that showed a bulk Curie temperature of 332 K. While the Curie temperature of Fe_5GeTe_2 is expected to decrease when the vdWs crystal is exfoliated into thin layers, the bulk value is still one of the highest recorded for a vdWs bulk magnet until now, making it an attractive 2D option to be used in spintronic devices. We used both VSM and FMR to study the magnetic properties of the Fe_5GeTe_2 sample. The experiments were performed with external magnetic fields applied along the c-axis and the ab-plane directions from 300 K to 10 K. We have focused on the temperature and field dependences of the g-factor and spin scattering mechanisms. The g-factor along the ab-plane is larger than that along the c-axis, indicative of considerable orbital momentum arising from spin-orbit coupling in Fe_5GeTe_2. The FMR analysis also reveals low temperature-enhanced linewidth broadening, together with the VSM data, they indicate a ferromagnetic to ferrimagnetic transition at lower T. For future studies, it will be interesting to exploit Fe_5GeTe_2 thin films for spin transport and spin-to-charge conversion experiments at room temperature. Fe_5GeTe_2 also opens new ways to build and study hybrid magnonic structures.

Acknowledgement

L.A. acknowledges the U.S. National Science Foundation (NSF) under grant No. DMR-2129879335 and Auburn University Research Support Program. L.B. is supported by the US DOE, Basic Enery Sciences program through award DE-SC0002613. A portion of this work was performed at the National High Magnetic Field Laboratory, which is supported by the National Science Foundation Cooperative Agreement No. DMR-1644779 and the State of Florida. A.R.M. and M.B. are supported by the U.S. Department of Energy, Office of Science, Basic Energy Sciences, Materials Sciences and Engineering Division. B.N. acknowledges support through NSF MEMONET grant #1939999, A.S. acknowledges support

NSF-CAREER Award #1452670, and P.L. acknowledges the Ralph E. Powe Junior Faculty Enhancement Award and valuable discussions with Prof. Mingzhong Wu, Prof. Satoru Emori, Prof. Wei Zhang, Dr. Chuanpu Liu, and Dr. Kaya Wei.

References

(1) Frisenda, R.; Niu, Y.; Gant, P.; Muñoz, M.; Castellanos-Gomez, A. Naturally occurring van der Waals materials. *npj 2D Materials and Applications* **2020**, *4*, 38.

(2) Mak, K. F.; Shan, J.; Ralph, D. C. Probing and controlling magnetic states in 2D layered magnetic materials. *Nature Reviews Physics* **2019**, *1*, 646–661.

(3) Mitta, S. B.; Choi, M. S.; Nipane, A.; Ali, F.; Kim, C.; Teherani, J. T.; Hone, J.; Yoo, W. J. Electrical characterization of 2D materials-based field-effect transistors. *2D Materials* **2020**, *8*, 012002.

(4) Casto, L. D.; Clune, A. J.; Yokosuk, M. O.; Musfeldt, J. L.; Williams, T. J.; Zhuang, H. L.; Lin, M.-W.; Xiao, K.; Hennig, R. G.; Sales, B. C.; Yan, J.-Q.; Mandrus, D. Strong spin-lattice coupling in CrSiTe3. *APL Materials* **2015**, *3*, 041515.

(5) Carteaux, V.; Brunet, D.; Ouvrard, G.; Andre, G. Crystallographic, magnetic and electronic structures of a new layered ferromagnetic compound Cr2Ge2Te6. *Journal of Physics: Condensed Matter* **1995**, *7*, 69–87.

(6) Tsubokawa, I. On the Magnetic Properties of a CrBr3 Single Crystal. *Journal of the Physical Society of Japan* **1960**, *15*, 1664–1668.

(7) McGuire, M. A.; Dixit, H.; Cooper, V. R.; Sales, B. C. Coupling of Crystal Structure and Magnetism in the Layered, Ferromagnetic Insulator CrI3. *Chemistry of Materials* **2015**, *27*, 612–620.

(8) Deiseroth, H.-J.; Aleksandrov, K.; Reiner, C.; Kienle, L.; Kremer, R. K. Fe3GeTe2 and Ni3GeTe2 – Two New Layered Transition-Metal Compounds: Crystal Structures, HRTEM Investigations, and Magnetic and Electrical Properties. *European Journal of Inorganic Chemistry* **2006**, *2006*, 1561–1567.

(9) Chen, B.; Yang, J.; Wang, H.; Imai, M.; Ohta, H.; Michioka, C.; Yoshimura, K.; Fang, M. Magnetic Properties of Layered Itinerant Electron Ferromagnet Fe3GeTe2. *Journal of the Physical Society of Japan* **2013**, *82*, 124711.

(10) Bander, M.; Mills, D. L. Ferromagnetism of ultrathin films. *Phys. Rev. B* **1988**, *38*, 12015–12018.

(11) Seo, J. et al. Nearly room temperature ferromagnetism in a magnetic metal-rich van der Waals metal. *Science Advances* **2020**, *6*.

(12) Deng, Y.; Yu, Y.; Song, Y.; Zhang, J.; Wang, N. Z.; Sun, Z.; Yi, Y.; Wu, Y. Z.; Wu, S.; Zhu, J.; Wang, J.; Chen, X. H.; Zhang, Y. Gate-tunable room-temperature ferromagnetism in two-dimensional Fe3GeTe2. *Nature* **2018**, *563*, 94–99.

(13) Li, Z.; Xia, W.; Su, H.; Yu, Z.; Fu, Y.; Chen, L.; Wang, X.; Yu, N.; Zou, Z.; Guo, Y. Magnetic critical behavior of the van der Waals Fe5GeTe2 crystal with near room temperature ferromagnetism. *Scientific Reports* **2020**, *10*, 15345.

(14) Zhu, J.-X.; Janoschek, M.; Chaves, D. S.; Cezar, J. C.; Durakiewicz, T.; Ronning, F.; Sassa, Y.; Mansson, M.; Scott, B. L.; Wakeham, N.; Bauer, E. D.; Thompson, J. D. Electronic correlation and magnetism in the ferromagnetic metal Fe_3GeTe_2. *Phys. Rev. B* **2016**, *93*, 144404.

(15) Verchenko, V. Y.; Tsirlin, A. A.; Sobolev, A. V.; Presniakov, I. A.; Shevelkov, A. V. Ferromagnetic Order, Strong Magnetocrystalline Anisotropy, and Magnetocaloric Effect in the Layered Telluride Fe3-δGeTe2. *Inorganic Chemistry* **2015**, *54*, 8598–8607, PMID: 26267350.

(16) May, A. F.; Ovchinnikov, D.; Zheng, Q.; Hermann, R.; Calder, S.; Huang, B.; Fei, Z.; Liu, Y.; Xu, X.; McGuire, M. A. Ferromagnetism Near Room Temperature in the Cleavable van der Waals Crystal Fe5GeTe2. *ACS Nano* **2019**, *13*, 4436–4442, PMID: 30865426.

(17) May, A. F.; Bridges, C. A.; McGuire, M. A. Physical properties and thermal stability of $Fe_{5-x}GeTe_2$ single crystals. *Phys. Rev. Materials* **2019**, *3*, 104401.

(18) Yamagami, K. et al. Itinerant ferromagnetism mediated by giant spin polarization of the metallic ligand band in the van der Waals magnet Fe_5GeTe_2. *Phys. Rev. B* **2021**, *103*, L060403.

(19) Zhang, H.; Chen, R.; Zhai, K.; Chen, X.; Caretta, L.; Huang, X.; Chopdekar, R. V.; Cao, J.; Sun, J.; Yao, J.; Birgeneau, R.; Ramesh, R. Itinerant ferromagnetism in van der Waals $Fe_{5-x}GeTe_2$ crystals above room temperature. *Phys. Rev. B* **2020**, *102*, 064417.

(20) Gao, Y.; Yin, Q.; Wang, Q.; Li, Z.; Cai, J.; Zhao, T.; Lei, H.; Wang, S.; Zhang, Y.; Shen, B. Spontaneous (Anti)meron Chains in the Domain Walls of van der Waals Ferromagnetic Fe5-xGeTe2. *Advanced Materials* **2020**, *32*, 2005228.

(21) Ohta, T.; Sakai, K.; Taniguchi, H.; Driesen, B.; Okada, Y.; Kobayashi, K.; Niimi, Y. Enhancement of coercive field in atomically-thin quenched Fe5GeTe2. *Applied Physics Express* **2020**, *13*, 043005.

(22) Oates, C.; Ogrin, F.; Lee, S.; Riedi, P.; Smith, G.; Thomson, T. High field ferromagnetic resonance measurements of the anisotropy field of longitudinal recording thin-film media. *Journal of Applied Physics* **2002**, *91*, 1417–1422.

(23) Shaw, J. M.; Nembach, H. T.; Silva, T. J.; Boone, C. T. Precise determination of the spectroscopic g-factor by use of broadband ferromagnetic resonance spectroscopy. *Journal of Applied Physics* **2013**, *114*, 243906.

(24) Lee, I.; Utermohlen, F. G.; Weber, D.; Hwang, K.; Zhang, C.; van Tol, J.; Goldberger, J. E.; Trivedi, N.; Hammel, P. C. Fundamental Spin Interactions Underlying the Magnetic Anisotropy in the Kitaev Ferromagnet CrI_3. *Phys. Rev. Lett.* **2020**, *124*, 017201.

(25) Zeisner, J.; Mehlawat, K.; Alfonsov, A.; Roslova, M.; Doert, T.; Isaeva, A.; Büchner, B.; Kataev, V. Electron spin resonance and ferromagnetic resonance spectroscopy in the high-field phase of the van der Waals magnet $CrCl_3$. *Phys. Rev. Materials* **2020**, *4*, 064406.

(26) Khan, S.; Zollitsch, C. W.; Arroo, D. M.; Cheng, H.; Verzhbitskiy, I.; Sud, A.; Feng, Y. P.; Eda, G.; Kurebayashi, H. Spin dynamics study in layered van der Waals single-crystal $Cr_2Ge_2Te_6$. *Phys. Rev. B* **2019**, *100*, 134437.

(27) Zhang, T.; Chen, Y.; Li, Y.; Guo, Z.; Wang, Z.; Han, Z.; He, W.; Zhang, J. Laser-induced magnetization dynamics in a van der Waals ferromagnetic Cr2Ge2Te6 nanoflake. *Applied Physics Letters* **2020**, *116*, 223103.

(28) Flovik, V.; Macià, F.; Kent, A. D.; Wahlström, E. Eddy current interactions in a ferromagnet-normal metal bilayer structure, and its impact on ferromagnetic resonance lineshapes. *Journal of Applied Physics* **2015**, *117*, 143902.

(29) Harder, M.; Cao, Z. X.; Gui, Y. S.; Fan, X. L.; Hu, C.-M. Analysis of the line shape of electrically detected ferromagnetic resonance. *Phys. Rev. B* **2011**, *84*, 054423.

(30) Mecking, N.; Gui, Y. S.; Hu, C.-M. Microwave photovoltage and photoresistance effects in ferromagnetic microstrips. *Phys. Rev. B* **2007**, *76*, 224430.

(31) Chang, H.; Li, P.; Zhang, W.; Liu, T.; Hoffmann, A.; Deng, L.; Wu, M. Nanometer-Thick Yttrium Iron Garnet Films With Extremely Low Damping. *IEEE Magnetics Letters* **2014**, *5*, 1–4.

(32) Rai, A.; Sapkota, A.; Pokhrel, A.; Li, M.; De Graef, M.; Mewes, C.; Sokalski, V.; Mewes, T. Higher-order perpendicular magnetic anisotropy and interfacial damping of Co/Ni multilayers. *Phys. Rev. B* **2020**, *102*, 174421.

(33) Kim, K. et al. Large anomalous Hall current induced by topological nodal lines in a ferromagnetic van der Waals semimetal. *Nature Materials* **2018**, *17*, 794–799.

(34) Costa, M.; Peres, N. M. R.; Fernández-Rossier, J.; Costa, A. T. Nonreciprocal magnons in a two-dimensional crystal with out-of-plane magnetization. *Phys. Rev. B* **2020**, *102*, 014450.

(35) Bruno, P. Tight-binding approach to the orbital magnetic moment and magnetocrystalline anisotropy of transition-metal monolayers. *Phys. Rev. B* **1989**, *39*, 865–868.

(36) Khodadadi, B.; Mohammadi, J. B.; Mewes, C.; Mewes, T.; Manno, M.; Leighton, C.; Miller, C. W. Enhanced spin pumping near a magnetic ordering transition. *Phys. Rev. B* **2017**, *96*, 054436.

(37) Kamberský, V. Spin-orbital Gilbert damping in common magnetic metals. *Phys. Rev. B* **2007**, *76*, 134416.

(38) Edwards, D. M. The absence of intraband scattering in a consistent theory of Gilbert damping in pure metallic ferromagnets. *Journal of Physics: Condensed Matter* **2016**, *28*, 086004.

(39) Costa, A. T.; Muniz, R. B. Breakdown of the adiabatic approach for magnetization damping in metallic ferromagnets. *Phys. Rev. B* **2015**, *92*, 014419.

(40) Jiang, S.; Sun, L.; Yin, Y.; Fu, Y.; Luo, C.; Zhai, Y.; Zhai, H. Ferromagnetic resonance linewidth and two-magnon scattering in Fe1-xGdx thin films. *AIP Advances* **2017**, *7*, 056029.

(41) Wang, Y.; Decker, M. M.; Meier, T. N. G.; Chen, X.; Song, C.; Grünbaum, T.; Zhao, W.; Zhang, J.; Chen, L.; Back, C. H. Spin pumping during the antiferromagnetic–ferromagnetic phase transition of iron–rhodium. *Nature Communications* **2020**, *11*, 275.

(42) Srivastava, A.; Singh, A. V.; Mohammadi, J. B.; Mewes, C.; Gupta, A.; Mewes, T. Ferromagnetic Resonance Study of the Verwey Phase Transition of Magnetite Thin Film on $MgGa_2O_4$(001) Substrate. *IEEE Transactions on Magnetics* **2020**, *56*, 1–6.

(43) Zhao, Y.; Song, Q.; Yang, S.-H.; Su, T.; Yuan, W.; Parkin, S. S. P.; Shi, J.; Han, W. Experimental Investigation of Temperature-Dependent Gilbert Damping in Permalloy Thin Films. *Scientific Reports* **2016**, *6*, 22890.

(44) Shen, X.; Chen, H.; Li, Y.; Xia, H.; Zeng, F.; Xu, J.; Kwon, H. Y.; Ji, Y.; Won, C.; Zhang, W.; Wu, Y. Multi-domain ferromagnetic resonance in magnetic van der Waals crystals CrI3 and CrBr3. *Journal of Magnetism and Magnetic Materials* **2021**, *528*, 167772.